catalysts

MDPI

Article

Highly Active $Mo_2C@WS_2$ Hybrid Electrode for Enhanced Hydrogen Evolution Reaction

Sajjad Hussain [1,2], Dhanasekaran Vikraman [3], Manzoor Hussain [2], Hyun-Seok Kim [3,*] and Jongwan Jung [1,2,*]

1 Hybrid Materials Center (HMC), Sejong University, Seoul 05006, Korea; shussainawan@gmail.com
2 Department of Nanotechnology and Advanced Materials Engineering, Sejong University, Seoul 05006, Korea; manzoorkacho186@gmail.com
3 Division of Electronics and Electrical Engineering, Dongguk University-Seoul, Seoul 04620, Korea; v.j.dhanasekaran@gmail.com
* Correspondence: hyunseokk@dongguk.edu (H.-S.K.); jwjung@sejong.ac.kr (J.J.)

Abstract: Transition metal dichalcogenides (TMDs) are the auspicious inexpensive electrocatalysts for the hydrogen evolution reaction (HER) which has been broadly studied owing to their remarkable enactment, however the drought of factors understanding were highly influenced to hinder their electrocatalytic behavior. Recently, transition metal carbide (TMC) has also emerged as an attractive electrode material due to their excellent ionic and electronic transport behavior. In this work, $Mo_2C@WS_2$ hybrids have been fabricated through a simple chemical reaction method. Constructed heterostructure electrocatalyts presented the small Tafel slope of 59 and 95 mV per decade and low overpotential of 93 mV and 98 @10 mA·cm^{-2} for HER in acidic and alkaline solution, respectively. In addition, 24-h robust stability with the improved interfacial interaction demonstrated the suitability of hybrid electrocatalyst for HER than their pure form of Mo_2C and WS_2 structures. The derived outcomes describe the generated abundant active sites and conductivity enhancement in TMC/TMD heterostructure along with the weaken ion/electron diffusion resistance for efficient energy generation applications.

Keywords: TMC; TMD; $Mo_2C@WS_2$; HER; H_2SO_4; KOH

check for updates

Citation: Hussain, S.; Vikraman, D.; Hussain, M.; Kim, H.-S.; Jung, J. Highly Active $Mo_2C@WS_2$ Hybrid Electrode for Enhanced Hydrogen Evolution Reaction. *Catalysts* **2021**, *11*, 1060. https://doi.org/10.3390/catal11091060

Academic Editors: Mohamed B. Zakaria, Ulf-Peter Apfel and Amir Pakdel

Received: 1 August 2021
Accepted: 30 August 2021
Published: 31 August 2021

1. Introduction

The swift development of global energy requirements and connected curb climate pollution, as well as environmental challenges has generated an imperative mandate to replace exhaustible fossil fuels for renewable energy sources. Hydrogen (H_2) is considered as a promising existent energy candidate for sustainable/environmental energy resources owing to their zero carbon emission and high energy density [1,2]. Currently, to obtain a superb H_2 evolution rate, the precious metals of Pt and, Pd based groups are considered as benchmark electrocatalysts for the hydrogen evolution reaction (HER) [1,2]. Due to the scarcity and high-cost, extensive efforts have been made to construct low-cost electrocatalysts, including transition metal carbide (TMC), transition metal chalcogenides (TMD), transition metal nitrides, and transition metal phosphides which have been performed well in acid or alkaline media [3–6]. The earth-abundant TMC have attracted tremendously by the research community due to low cost, easy availability and active and stable HER characteristics in both acidic and base medium [7]. Amongst, Mo_2C has considered as promising a substitutes for expensive Pt-based catalysts resembling that of Pt-like electronic structure, high corrosion resistance and superior electrical conductivity (~1.0×10^2 S·cm^{-1}) [8]. Due to the aggregation/entanglement and coalescence of nanoparticles and low surface areas, bare Mo_xC nanoparticles toward HER are considered as a premature electrocatalysts. Various nanocarbons (carbon nanotubes, graphene, or graphene oxide) are connected/blended with Mo_xC to prevent aggregation and propagation of active nanoparticles. TMDs have

the chemical composition of MX_2 (M-Metal and X- chalcogen elements) with lamellar sandwich structure. TMDs layered bulk structure own the covalent bonds between M atoms and X atoms, whereas the layers of TMDs are bound to each other by weak van der Waals forces. Among the various TMD candidates, WS_2 is a highly favorable member for HER applications. Theoretical and experimental assumptions also confirm that the active electrocatalytic sites of WS_2 are primarily situated on metallic edges, whereas the basal surfaces are catalytically inert [9]. Due to large amount of edge sites, easy ion transport channel and large specific surface area of WS_2 have been broadly opened their use as HER catalysts. By taking advantage of numerous pores, edges shape architecture, and modifiable active interface of TMD or TMC, fabrication of TMD/TMC hybridize material is still appealing by research community. However, the study of TMD/TMC based hybrid for HER application is still infancy and there are only few articles deal with this topic. Quite recently, TMD/TMC has proven to be a powerful method to enhance the electrocatalytic activity, such as MoS_2/Mo_2C hybrid nanosheets [10], $W_xC@WS_2$ nanostructure [11], WS_2/W_2C hybrid [12,13], Ni-induced nitrogen-doped carbon@$Mo_2C@MoS_2$ [14], $MoSe_2$-Mo_2C hybrid [15], 3D $Mo_2C@MoS_2$ heterojunction [16], $MoS_2@X_2C$ (X = Mo or W) hybrids [17].

The combination of both TMD/TMC structure present several advantages: (1) Mo_2C act as substrate and blended WS_2 nanomaterial consciously avoided the aggregation/restacking of Mo_2C; (2) defect-rich TMD nanosheets or introduction of sulfur (S) vacancy defects activates the WS_2 basal plane and creates the plentiful active sites [16]; (3) TMC improves surface area, conductivity and durability of the electrocatalysts, and also expands the interlayer spacing between TMD and TMC sheets, enables the transmission of mass/charge and reduces the diffusion resistance of ions in the electrode; (4) porous active structures weaken the diffusion resistance, reduce the interfacial contact resistance and promote the interface charge transfer; (5) hybrid improves the activity and reduces the Gibbs hydrogen adsorption free energy (ΔG_H) due to strong chemical binding and electrical coupling between 2D conductive networks [17]. Thus, the intrinsic catalytic property of WS_2 material has vital role. However, controlled growth of TMD/TMC hybrid via rationally designed architecture for an effective HER performance is still a challenge. Previously, our group have prepared MoS_2/Mo_2C and WS_2/W_2C based hybrids for various electrochemical applications [13,17]. However, this work is focused to form the dissimilar structures interacted $WS_2@Mo_2C$ hybrid for the enhanced HER characteristics. In this report, we combined a chemical reaction and carburization method which was adopted to synthesize vertical $Mo_2C@WS_2$ nanosheets for HER application. $Mo_2C@WS_2$ hybrid electrode offers a low overpotential of 59 and 95 mV in acidic and alkaline medium, respectively, lower than the respective pure WS_2 and Mo_2C electrodes.

2. Experimental Section

Synthesis of $Mo_2C@WS_2$ Hybrid

Mo_2C (Commercial −325 mesh, 99.5%; CAS Number: 12069-89-5, Sigma-Aldrich, Gangnam-Gu, Seoul, Korea) powder was used to synthesize the reduced Mo_2C nanoparticles, as reported earlier [18,19]. The commercial Mo_2C powder was liquefied in ethanol blended ammonia, and then boiled under vigorous agitation using hot plate at 85 °C for 5 h. After cleansing with deionized (DI) water and ethanol via centrifugation, the ensuing blend was dried in an oven at 80 °C overnight. To finish, the ensuing dark powder was collected and then post-annealed at 850 °C under a gaseous mixture of Ar (30 sccm), H_2 (30 sccm) and CH_4 (30 sccm) for 3 h. A simple hydrothermal method was adopted to synthesis of WS_2 nanoparticle. All the chemicals were purchased from Merck Korea, Gangnam-Gu, Seoul, Korea. Typically, 0.003 mol of sodium tungstate ($Na_2WO_4{\cdot}2H_2O$), 0.01 mol of hydroxylamine hydrochloride ($NH_2OH{\cdot}HCl$) and 0.008 mol of thiourea (CH_4N_2S)) were dissolved in 50 mL deionized water under vigorous magnetic stirring. Hydrochloric acid (HCl) and ammonia water ($NH_3{\cdot}H_2O$) were added stepwise to control the PH value to 6. The final solution was transferred into a 100 mL Teflon steel chamber, sealed into an autoclave

and incubated tightly, heated at 180 °C for 12 h and then naturally cooled down to room temperature. The black precipitates were recovered from the solution by centrifugation (5000 rpm, 10 min) and cleansed with ethanol and DI water several times, lastly dehydrated in vacuum for 12 h at 80 °C.

For $Mo_2C@WS_2$ nanosheets synthesis, the commercial Mo_2C powder was firstly dispersed into ethanol (100 mL). Next, a mixture of $Na_2WO_4{\cdot}2H_2O$ (0.01 mol), $NH_2OH{\cdot}HCl$ (0.003 mol) and CH_4N_2S (0.008 mol) were added in 100 mL DI water separately, then calibrated to PH value 6 by dissolving the HCl and $NH_3{\cdot}H_2O$. After the dispersion, Mo_2C were poured into WS_2 mixture at room temperature with continuous magnetic agitation. The intermediate blended solution was transferred to an autoclave. Furthermore, it was also sealed and heated at 200 °C for 12 h, then allowed cooling to room temperature. The dark solution was then cleaned with DI water and ethanol using a centrifuge, then dried overnight at 100 °C. Finally, the prepared black powders were annealed for 1 h at 850 °C in tubular furnace under a blended gas of $H_2/Ar/CH_4$. The detailed characterization information is provided in the supporting information.

3. Results and Discussion

The process for preparation of $Mo_2C@WS_2$ hybrid via one-step chemical treatment is illustrated in Figure 1. Raman spectroscopy was used to understand the structural properties of Mo_2C, WS_2 and $Mo_2C@WS_2$ hybrid. Figure 2a shows the Raman profiles of prepared nanostructures. The pure Mo_2C yields three well-documented Raman shifts at 662 cm^{-1}, 817 cm^{-1}, and 990 cm^{-1} consents to the Mo_2C formation. For WS_2, two pronounced peaks centered at 350 and 420 cm^{-1}, can be assigned to E_{2g} and A_{1g} modes, respectively. From $Mo_2C@WS_2$ hybrid, both Mo_2C and WS_2 phase peaks are presented which suggesting the formation of $Mo_2C@WS_2$ heterogeneous structure. In addition, $Mo_2C@WS_2$ heterostructure produces the low intensity peaks at 132 cm^{-1} and 259 cm^{-1} region corresponds to J_1, and A_g mode 1T′ phase WS_2, respectively [20,21]. The slight peak shift might be a substantial amount of diffusion of C and S elements on W/Mo sides. Figure 2b shows the X-ray diffraction (XRD) profiles of Mo_2C, WS_2 and $Mo_2C@WS_2$ hybrid. The prepared Mo_2C reveals (201), (112), (103), (110), (102), (002) and (100) lattice planes along with (101) preferential orientation, which are indexed with a standard result (JCPDS–893014). The diffraction pattern from WS_2 nanosheets contains peak from (002), (004), (006), and (008) lattices, correlated with a standard result (JCPDS–080237). For $Mo_2C@WS_2$ hybrid, the amalgamated peaks from Mo_2C and WS_2 are observed which indicated the highly effective preparation for hybrid structure.

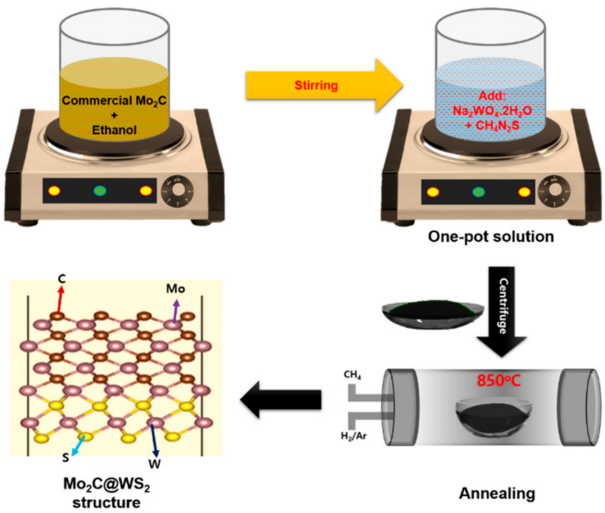

Figure 1. Schematic illustration for the $Mo_2C@WS_2$ hybrid preparation.

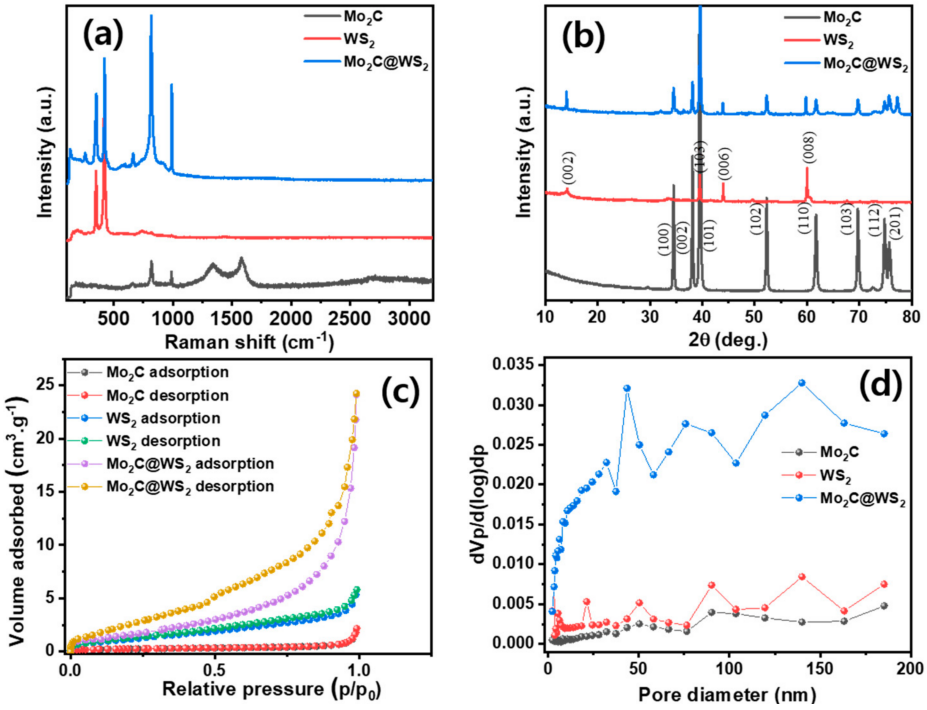

Figure 2. (**a**) Raman spectra and (**b**) XRD patterns (**c**) Nitrogen isotherm curves and (**d**) pore diameter variations for Mo_2C, WS_2 and $Mo_2C@WS_2$ hybrids.

The Brunauer–Emmett–Teller (BET) surface area analysis and its pore size distribution of Mo_2C, WS_2 and $Mo_2C@WS_2$ hybrid were ascertained by the N_2 adsorption−desorption measurements. Figure 2c represents the BET sorption profiles for Mo_2C, WS_2 and $Mo_2C@WS_2$ hybrid. The improved BET area of 7.49 $m^2 \cdot g^{-1}$ was retrieved for the $Mo_2C@WS_2$ hybrid, which is larger than that of WS_2 (4.24 $m^2 \cdot g^{-1}$) and Mo_2C (0.83 $m^2 \cdot g^{-1}$). Furthermore, the pore diameter in terms of pore volume profile (Figure 2d) depicts the mesoporous behavior of Mo_2C, WS_2, and $Mo_2C@WS_2$ with the pore diameter of 14.3, 8.01, and 19.1 nm, and the pore volume of 0.00297, 0.00741, and 0.0357 $cm^3 \cdot g^{-1}$, respectively.

Furthermore, field emission scanning electron microscopy (FESEM) was used to analyze the surface modification of prepared nanostructures. Figure 3a–c displays the Mo_2C nanostructures FESEM images. The observation demonstrates the accumulated bulk structure grains which lump of spherical shaped nanoparticles. Figure 3d–f represents the FESEM images with different magnifications for WS_2 nanostructures. WS_2 also exposes the grain bunches through agglomerated nanoparticles. The prepared $Mo_2C@WS_2$ hybrids FESEM images are clearly pictured the formation bulk grains by the agglomerated nanoparticles as shown in the Figure 3g–i. The elemental mapping was performed for $Mo_2C@WS_2$ hybrids (Figure S1) to confirm the spatial distribution of Mo, W, C and S elements. The observed results are confirmed the uniform distribution of all the elements in the $Mo_2C@WS_2$ heterostructure.

Furthermore, X-ray photoelectron spectral (XPS) analysis was done to evaluate the chemical composition and electronic structures of $Mo_2C@WS_2$ hybrid electrocatalyst. Figure 4a displays the survey profile of $Mo_2C@CNT$ hybrid. Figure 4b presents the W 4f binding energy spectrum for hybrid. The deconvoluted spectrum clearly exposes the W $4f_{7/2}$ and W $4f_{5/2}$ characteristic peaks along with $5p_{3/2}$ peak [22]. Figure 4c displays the S 2p region which establishes the $2p_{3/2}$ and $2p_{1/2}$ doublets [22]. The C 1s profile (Figure 4d) shows a strong peak due to C–C relation in Mo_2C at 284.5 eV binding energy with the shoulder peaks at 283.5 and 286.4 eV due to Mo–C and C–O, respectively [7,23,24]. The high-resolution Mo 3d region (Figure 4e) exposes the peak at 228.3 eV and 231.6 eV ascribes to the Mo^{2+} $3d_{5/2}$ and Mo^{2+} $3d_{3/2}$, respectively for $Mo_2C@WS_2$ hybrid [15,25]. In addition, the strong bands related to Mo^{4+} $3d_{5/2}$ and Mo^{4+} $3d_{3/2}$ along with Mo^{6+} are observed for

hybrid structure [26–30]. The presence of Mo^{4+} states indicates interaction of sulfur [17]. Hence, the observed results are clearly proved the hybrid formation.

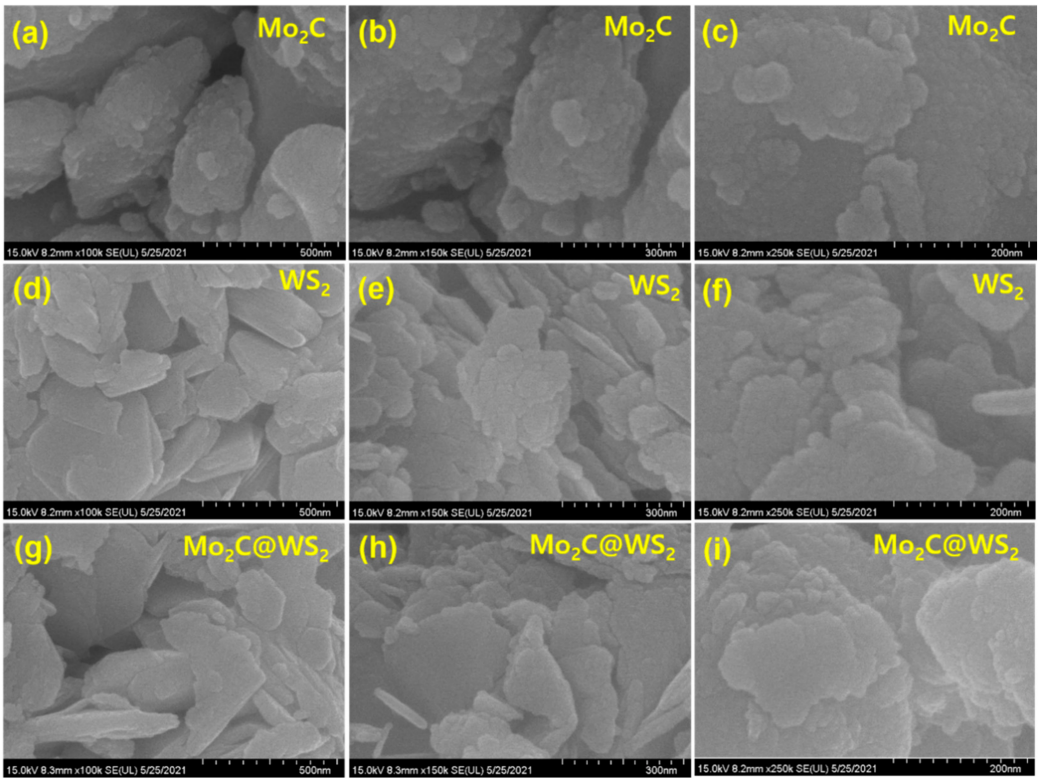

Figure 3. FESEM images for (**a**–**c**) Mo_2C; (**d**–**f**) WS_2 and (**g**–**i**) $Mo_2C@WS_2$.

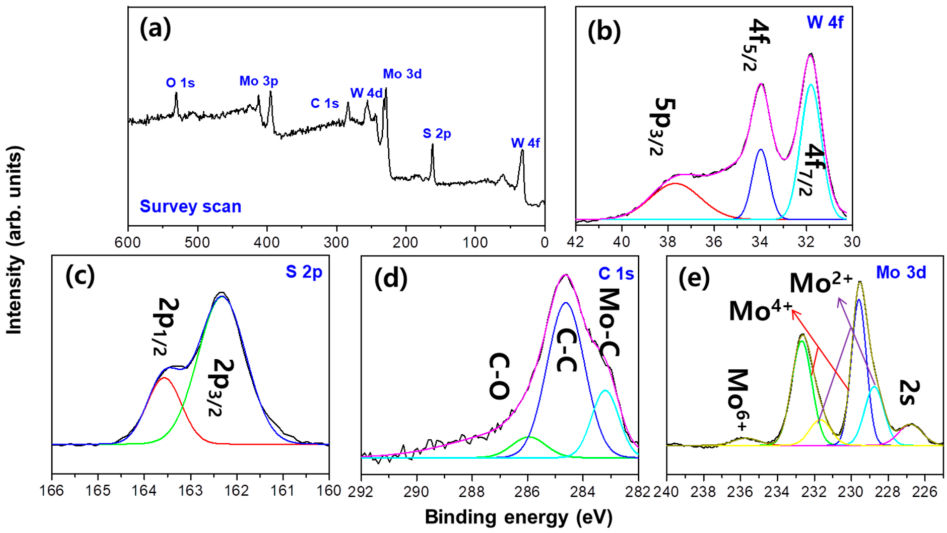

Figure 4. XPS spectra of the $Mo_2C@WS_2$ hybrids: (**a**) survey scan; (**b**) W 4f; (**c**) S 2p; (**d**) C 1s and (**e**) Mo 3d binding energy.

Figure 5 represents the different magnifications of transmission electron microscopy (TEM) images for $Mo_2C@WS_2$ hybrid. A low magnification TEM image obviously reveals the decorated sheet like vertically aligned intersected layers (Figure 5a). Figure 5b,c reveal the exhibit of nano-fringes interaction with the vertically aligned layers. The high magnification images also clearly represent the well interaction between the Mo_2C and WS_2, which are outlined, in the hybrid structure. Figure 5d shows the FFT profile which proves crystalline direction of Mo_2C and WS_2 in the hybrid. Figure 5e shows the phase spectrum

which reveals the 0.237 nm lattice spacing due to the (002) plane of Mo_2C with their inserted inverse FFT profile. Figure 5f explores phase profile of WS_2 (002) lattice direction with a spacing of 0.615 nm. The perceived highly interfaced fingerprint structures with the vertically aligned nano-stripes would be greatly supported to achieve the improved electrochemical characteristics [17,31].

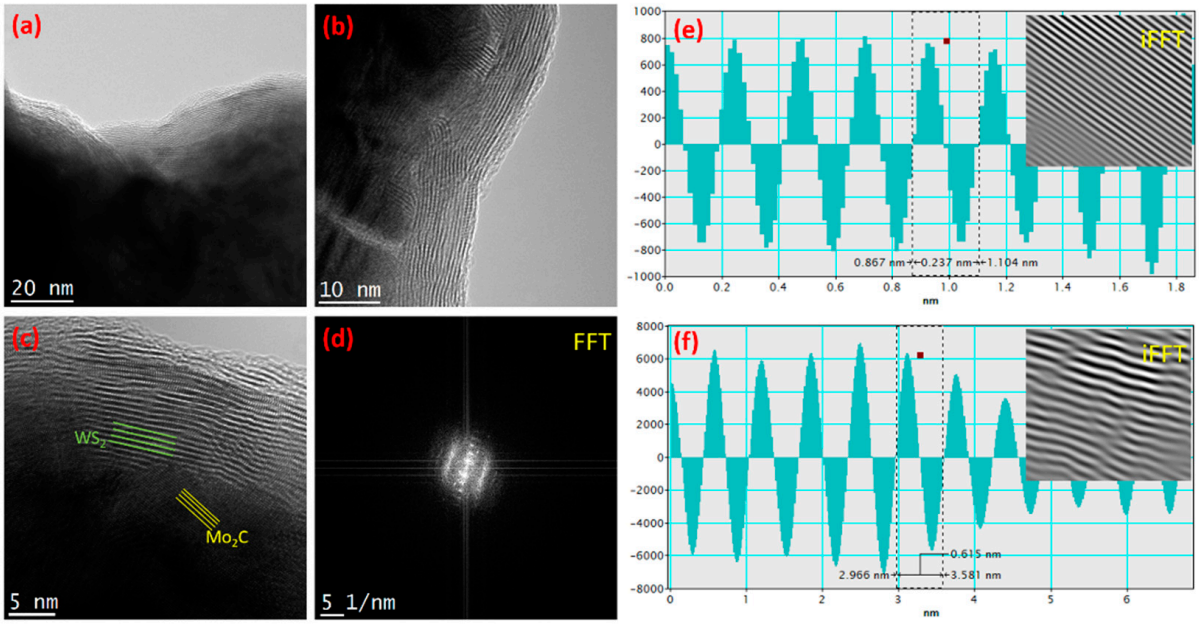

Figure 5. TEM images of $Mo_2C@WS_2$ hybrid: (**a**) low and (**b**,**c**) high-resolution images (yellow line indicates the Mo_2C fringes and green line indicates the WS_2 layers); (**d**) FFT pattern and (**e**,**f**) phase profiles for the (**e**) Mo_2C (002) and (**f**) WS_2 (002) lattice directions (inset: corresponding inverse FFT profile).

The electrocatalytic performance of all catalysts (Pt/C, Mo_2C, WS_2 and $Mo_2C@WS_2$ hybrid) for HER were assessed using a standard three-electrode configuration using N_2-saturated 0.5 M H_2SO_4 and 1.0 M KOH electrolyte at room temperature. The active loading mass of materials was 2 mg·cm^{-2}. The polarization curves were collected from the iR-compensated linear sweep voltammetry (LSV) measurements at 10 mV·s^{-1}. Figure 6a,b show the polarization profiles for Pt/C, Mo_2C, WS_2 and $Mo_2C@WS_2$ hybrid in acidic and alkaline media, respectively. As expected, the commercial Pt/C has outstanding HER performance with an overpotential of 48 and 45 mV vs RHE, respectively to reach 10 mA·cm^{-2} in acidic and alkaline medium. The hybrid $Mo_2C@WS_2$ catalyst produces a superior electrocatalytic performance with a overpotential of 93 mV compared to the Mo_2C (134 mV) and WS_2 (126 mV) mono-component in acidic medium. Likewise, the overpotentials of bare NF, Mo_2C, WS_2, and $Mo_2C@WS_2$ hybrid were 430, 116, 108, and 98 mV vs RHE achieving a current density of 10 mA·cm^{-2} in alkaline solution, respectively (Figure 6b). The observed result is better than most of TMD and TMC based HER catalysts in acidic and alkaline medium (Table S1), such as W_2C/WS_2 hybrid ~133 and 105 mV@10 mA·cm^{-2} [13], MoC-Mo_2C hetero nanowires ~126 & 120@ 10 mA·cm^{-2} [32], MoC_x nano-octahedrons ~142 & 151@ 10 mA·cm^{-2} [33], MoS_2/Mo_2C-NCNTs~145@ 10 mA·cm^{-2} and MoS_2/WSe_2 heterostructures ~116@ 10 mA·cm^{-2} in acidic medium [34]. The excellent performance of HER could be attributed by the highly active edge site of WS_2 and superior conductivity of Mo_2C or partial substitution of C/S atom owing to heterostructure formed by the mutual coordination between WS_2 and Mo_2C.

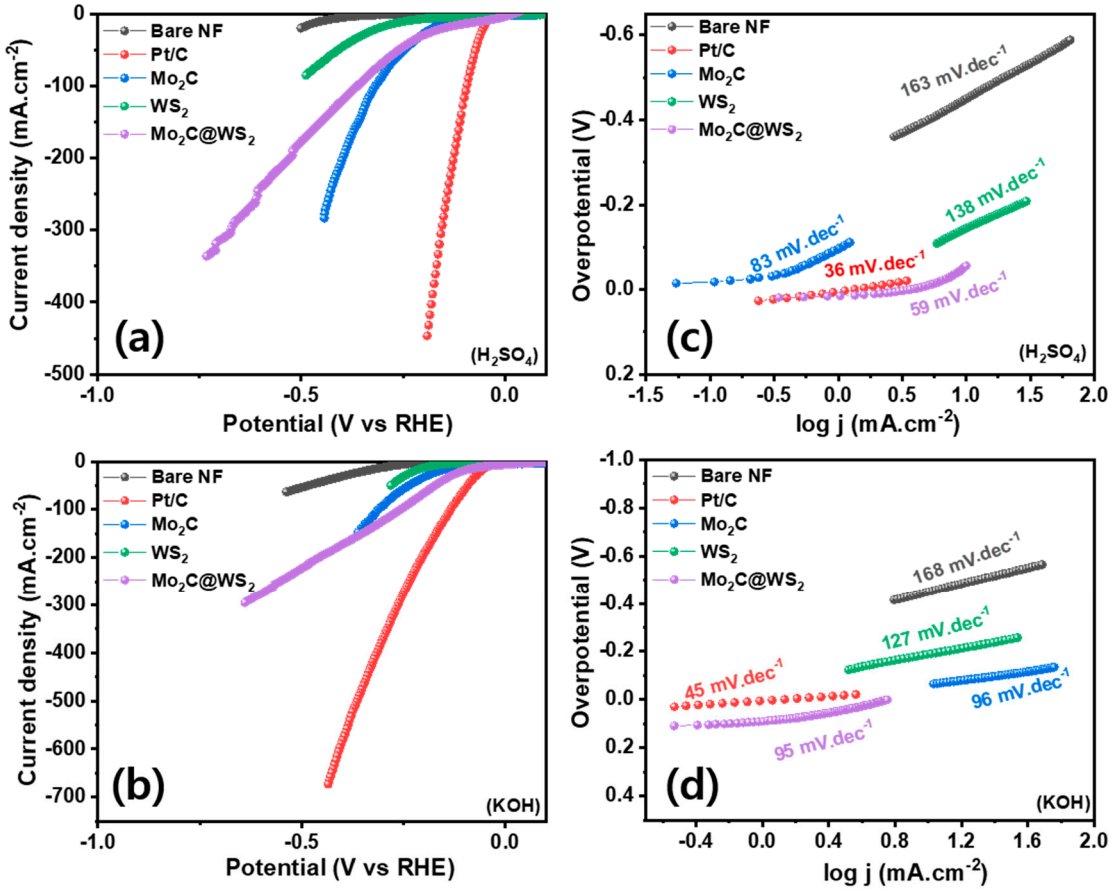

Figure 6. Hydrogen evolution: LSV curves for Pt/C, bare NF, Mo_2C, WS_2 and Mo_2C @ WS_2 hybrid at sweep rate of 10 mV·s^{-1} (**a**) 0.5 M H_2SO_4 (**b**) 1 M KOH; Tafel plots for Pt/C, bare NF, Mo_2C, WS_2 and $Mo_2C@WS_2$ hybrid (**c**) 0.5 M H_2SO_4 and (**d**) 1 M KOH.

To illustrate the internal HER kinetic reaction mechanism, the Tafel plots were derived from its respective LSV profiles. The linear portion of Tafel plots are mounted to extract the Tafel slopes as shown in the Figure 6c,d. The observed slope values are at 36, 83, 138, 59 and 163 mV per decade for Pt/C, Mo_2C, WS_2, $Mo_2C@WS_2$ hybrid and bare NF, respectively in acid medium. In an alkaline medium, Tafel slopes of 45, 96, 127, 95, and 168 mV·dec^{-1} were found Pt/C, Mo_2C, WS_2, $Mo_2C@WS_2$ hybrid and bare NF, respectively. Extensively described HER processes are implicated in the alkaline and acidic electrolyte, which follows by the leading release of H_3O^+ and H_{ads} creation [35–37]. The following three phases of HER process is defined in acid media.

$$\text{Herrovsky}: \; H_{ads} + H_3O^+ + e^- \rightarrow H_{2\uparrow} + H_2O \tag{1}$$

$$\text{Volmer}: \; H_3O^+ + e^- \rightarrow H_{ads} + H_2O \tag{2}$$

$$\text{Tafel}: \; H_{ads} + H_{ads} \rightarrow H_{2\uparrow} \tag{3}$$

HER kinetics is defined by subsequent phases in an alkaline solution:

$$\text{Herrovsky}: \; H_2O + e^- + H_{ads} \rightarrow H_{2\uparrow} + OH^- \tag{4}$$

$$\text{Volmer}: \; H_2O + e^- \rightarrow H_{ads} + OH^- \tag{5}$$

$$\text{Tafel}: \; 2H_{ads} \rightarrow H_{2\uparrow} \tag{6}$$

Furthermore, the 59 and 95 mV·dec^{-1} Tafel slope for $Mo_2C@WS_2$ hybrid suggests that the rate-determining step may be designated as an electrochemical desorption mechanism (Volmer−Heyrovsky kinetics reaction). To evaluate the inherent catalytic yield

of Mo_2C, WS_2, and the $Mo_2C@WS_2$ hybrid, the exchange current density (j_0) was also studied by extrapolating from the Tafel plots. The normalized j_0 value of $Mo_2C@WS_2$ (1.54 and 1.19 mA·cm^{-2}) is superior than Mo_2C (0.13 and 0.93 mA·cm^{-2}) and WS_2 (0.83 and 0.91 mA·cm^{-2}) for acidic and alkaline media, which signifying an enhanced rates of intrinsic electron transference among the catalyst and the electrolyte. The electrochemical impedance spectroscopy (EIS) study was implemented to understand the boundary reactions and electrode charge transport kinetics for HER. Figure 7a,b show Nyquist graphs of Mo_2C, WS_2, and the $Mo_2C@WS_2$ hybrid electrocatalysts in acid and base solution, respectively (inset equivalent circuit). The smaller R_{ct} value of the $Mo_2C@WS_2$ hybrid (~2.98 Ω & 2.08 Ω) electrocatalysts substantially boost the interfacial electron/ion diffusion compared to Mo_2C (~3.4 Ω & 4.1 Ω) and WS_2 (~3.3 Ω & 3.9 Ω) in acid and base media. The low R_{ct} of $Mo_2C@WS_2$ hybrid may be related to effect of intimate contact effect between the exposed edges sites (WS_2) and the reaction of the metallic superconductor Mo_2C sublayers that can reduce the resistance to electron transportation at the porous catalyst/electrolyte boundary and then produce the rapid response for HER. The observed electrochemical HER parameters are provided in the Table S1, supporting information.

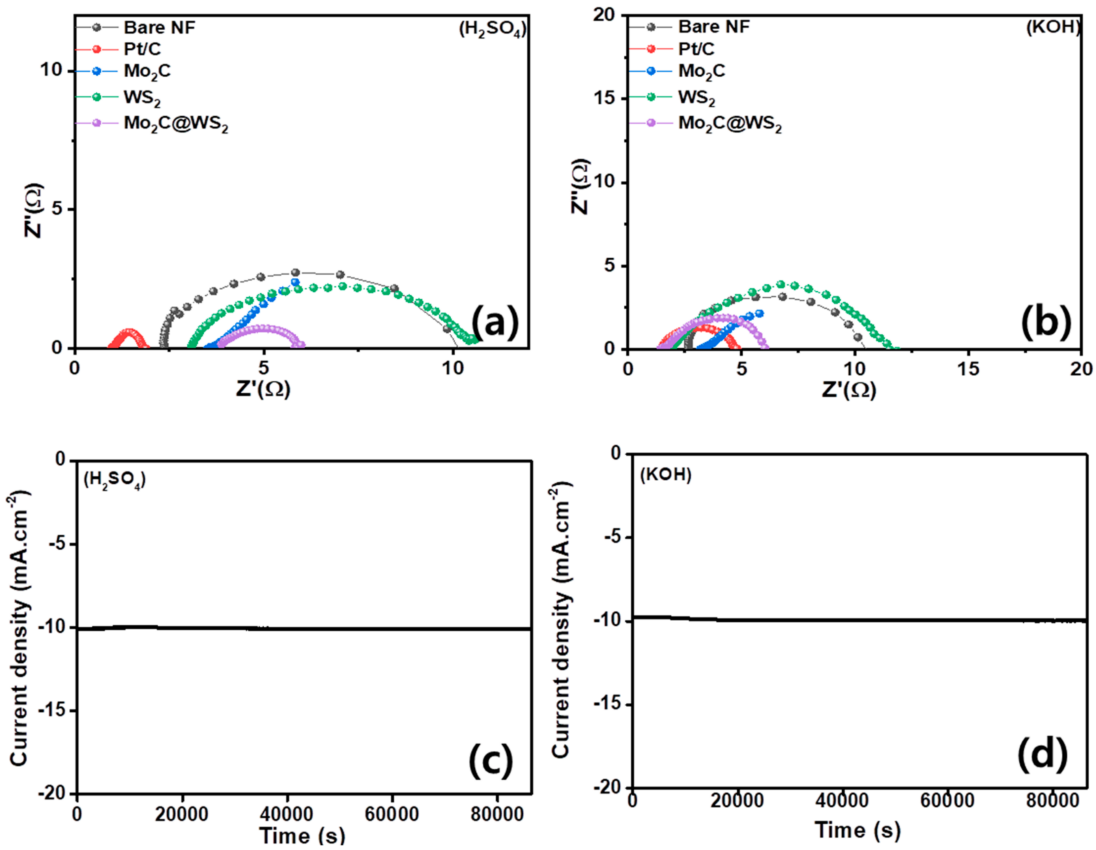

Figure 7. EIS profiles for Pt/C, bare NF, Mo_2C, WS_2 and Mo_2C @ WS_2 hybrid (**a**) 0.5M H_2SO_4 and (**b**) 1 M KOH; Chronoamperometric profile at constant overpotential (**c**) 0.5 M H_2SO_4 and (**d**) 1 M KOH.

Long-term robustness is another critical parameter of electrocatalysts for HER application. The long-term durability of $Mo_2C@WS_2$ and the ability to constantly catalyze H_2 production was tested in 24-h continuous chronoamperometric process in acid and base medium using constant potential of 93 mV and 98 mV vs RHE, respectively. Figure 7c displays the chronoamperometric curves of the $Mo_2C@WS_2$ electrocatalyst in the acidic medium. No significant loss of cathodic current density occurred over 24-h of electrolysis in an acidic medium, which implies stable performance with high charge transportation capability between $Mo_2C@WS_2$ hybrid. Figure 7d depicted the chronoamperometric curves (i-t) in the base electrolyte for the $Mo_2C@WS_2$ electrocatalyst. Slight degradation cathodic

current density was observed due to the formation of H_2 bubble over 24-h of electrolysis in the base medium. For the HER reaction of $Mo_2C@WS_2$ hybrid, TMD WS_2 is a dominant supplier of active sites. During the HER reaction mechanism, the catalytic active sites of WS_2 are supposed to be moved to the terraces from the chalcogens under alkaline conditions, whereas the dominant active facets are shifted to edge sites in acid media [38]. These sensitive edge sites are more active than the oblivious terrace sites, thereby acidic medium offers the improved HER behavior rather than alkaline media [38,39]. The hybrid HER results are compared with the $Mo_2C@WS_2$ outcomes in Table S2. Furthermore, FESEM studies were performed to explore the stability of prepared $Mo_2C@WS_2$ hybrid after 24-h continuous operation which clearly proves their robust nature without any structural alteration/collapse as represented in Figure S2.

4. Conclusions

In this report, vertical $Mo_2C@WS_2$ nanosheets were synthesized by chemical reaction and carburization method. The constructed $Mo_2C@WS_2$ heterostructure was evidently confirmed by the Raman, XRD, XPS, FESEM and TEM studies. The prepared hybrid electrocatalyst revealed the low overpotential of 93 and 98 mV at 10 mA·cm^{-2} and Tafel slope of 59 and 95 mV per decade in acidic and alkaline medium, respectively, outperforming the performance of pristine WS_2 and Mo_2C under the same condition. The robust stability was observed over 24-h HER operation under alkaline and acidic medium by $Mo_2C@WS_2$ hybrid electrocatalyst. This work highlights a new path to regulate the WS_2 based hybrid material through facile and economical approach for the enhanced HER activity.

Supplementary Materials: The following are available online at https://www.mdpi.com/article/10.3390/catal11091060/s1, Figure S1: (a) Elemental mapping image of $Mo_2C@WS_2$ hybrid and their individual elements distribution; (b) Mo; (c) C; (d) S and (e) W; Figure S2: FESEM images for $Mo_2C@WS_2$ hybrid after the 24-h continuous HER process in acid medium, Table S1: Comparison of electrochemical parameters for different electrocatalysts, Table S2: HER catalytic performances TMDs and TMCs-based electrocatalysts.

Author Contributions: Conceptualization, S.H. and J.J.; Data curation, D.V. and M.H.; Formal analysis, S.H. and M.H.; Investigation, D.V. and H.-S.K.; Methodology, S.H.; Resources, H.-S.K.; Supervision, J.J.; Validation, H.-S.K.; Writing—original draft, S.H.; Writing—review and editing, D.V., H.-S.K. and J.J. All authors have read and agreed to the published version of the manuscript.

Funding: This research was supported by the Nano Material Technology Development Program and Basic Science Research Program through the National Research Foundation of Korea (NRF) funded by the Ministry of Education, and the Science and ICT (2016M3A7B4909942, 2017R1C1B5076952, 2016R1D1A1B01015047, and NRF-2020R1A6A1A03043435).

Data Availability Statement: Not applicable.

Conflicts of Interest: The authors declare no conflict of interest.

References

1. Dresselhaus, M.; Thomas, I. Alternative energy technologies. *Nature* **2001**, *414*, 332–337. [CrossRef]
2. Turner, J.A. Sustainable hydrogen production. *Science* **2004**, *305*, 972–974. [CrossRef] [PubMed]
3. Vikraman, D.; Hussain, S.; Rabani, I.; Feroze, A.; Ali, M.; Seo, Y.-S.; Chun, S.-H.; Jung, J.; Kim, H.-S. Engineering $MoTe_2$ and janus semote nanosheet structures: First-principles roadmap and practical uses in hydrogen evolution reactions and symmetric supercapacitors. *Nano Energy* **2021**, *87*, 106161. [CrossRef]
4. Zou, X.; Zhang, Y. Noble metal-free hydrogen evolution catalysts for water splitting. *Chem. Soc. Rev.* **2015**, *44*, 5148–5180. [CrossRef] [PubMed]
5. Xiao, P.; Chen, W.; Wang, X. A review of phosphide-based materials for electrocatalytic hydrogen evolution. *Adv. Energy Mater.* **2015**, *5*, 1500985. [CrossRef]
6. Theerthagiri, J.; Lee, S.J.; Murthy, A.P.; Madhavan, J.; Choi, M.Y. Fundamental aspects and recent advances in transition metal nitrides as electrocatalysts for hydrogen evolution reaction: A review. *Curr. Opin. Solid State Mater. Sci.* **2020**, *24*, 100805. [CrossRef]

7. Hussain, S.; Vikraman, D.; Feroze, A.; Song, W.; An, K.-S.; Kim, H.-S.; Chun, S.-H.; Jung, J. Synthesis of Mo_2C and W_2C nanoparticle electrocatalysts for the efficient hydrogen evolution reaction in alkali and acid electrolytes. *Front. Chem.* **2019**, *7*, 716. [CrossRef] [PubMed]
8. Miao, M.; Pan, J.; He, T.; Yan, Y.; Xia, B.Y.; Wang, X. Molybdenum carbide-based electrocatalysts for hydrogen evolution reaction. *Chem. Eur. J.* **2017**, *23*, 10947–10961. [CrossRef]
9. Lukowski, M.A.; Daniel, A.S.; English, C.R.; Meng, F.; Forticaux, A.; Hamers, R.J.; Jin, S. Highly active hydrogen evolution catalysis from metallic WS_2 nanosheets. *Energy Environ. Sci.* **2014**, *7*, 2608–2613. [CrossRef]
10. Zhao, Z.; Qin, F.; Kasiraju, S.; Xie, L.; Alam, M.K.; Chen, S.; Wang, D.; Ren, Z.; Wang, Z.; Grabow, L.C. Vertically aligned MoS_2/Mo_2C hybrid nanosheets grown on carbon paper for efficient electrocatalytic hydrogen evolution. *ACS Catal.* **2017**, *7*, 7312–7318. [CrossRef]
11. Wang, F.; He, P.; Li, Y.; Shifa, T.A.; Deng, Y.; Liu, K.; Wang, Q.; Wang, F.; Wen, Y.; Wang, Z. Interface engineered $W_xC@WS_2$ nanostructure for enhanced hydrogen evolution catalysis. *Adv. Funct. Mater.* **2017**, *27*, 1605802.
12. Li, Y.; Wu, X.; Zhang, H.; Zhang, J. Interface designing over WS_2/W_2C for enhanced hydrogen evolution catalysis. *ACS Appl. Energy Mater.* **2018**, *1*, 3377–3384. [CrossRef]
13. Hussain, S.; Rabani, I.; Vikraman, D.; Feroze, A.; Ali, M.; Seo, Y.-S.; Kim, H.-S.; Chun, S.-H.; Jung, J. One-pot synthesis of w_2c/ws_2 hybrid nanostructures for improved hydrogen evolution reactions and supercapacitors. *Nanomaterials* **2020**, *10*, 1597. [CrossRef] [PubMed]
14. Gong, L.; Mu, X.; Li, Q.; Ma, L.; Xiong, Y.; Li, R. Rational design of ni-induced $NC@Mo_2C@MoS_2$ sphere electrocatalyst for efficient hydrogen evolution reaction in acidic and alkaline media. *Int. J. Hydrogen Energy* **2021**, *46*, 5250–5258. [CrossRef]
15. Vikraman, D.; Hussain, S.; Karuppasamy, K.; Feroze, A.; Kathalingam, A.; Sanmugam, A.; Chun, S.-H.; Jung, J.; Kim, H.-S. Engineering the novel $MoSe_2$-Mo_2C hybrid nanoarray electrodes for energy storage and water splitting applications. *Appl. Catal. B* **2020**, *264*, 118531. [CrossRef]
16. Yang, S.; Wang, Y.; Zhang, H.; Zhang, Y.; Liu, L.; Fang, L.; Yang, X.; Gu, X.; Wang, Y. Unique three-dimensional $Mo_2C@MoS_2$ heterojunction nanostructure with s vacancies as outstanding all-ph range electrocatalyst for hydrogen evolution. *J. Catal.* **2019**, *371*, 20–26. [CrossRef]
17. Hussain, S.; Rabani, I.; Vikraman, D.; Feroze, A.; Ali, M.; Seo, Y.-S.; Song, W.; An, K.-S.; Kim, H.-S.; Chun, S.-H.; et al. $MoS_2@X_2C$ (x = Mo or W) hybrids for enhanced supercapacitor and hydrogen evolution performances. *Chem. Eng. J.* **2021**, *421*, 127843. [CrossRef]
18. Faizan, M.; Hussain, S.; Vikraman, D.; Ali, B.; Kim, H.-S.; Jung, J.; Nam, K.W. $MoS_2@Mo_2C$ hybrid nanostructures formation as an efficient anode material for lithium-ion batteries. *J. Mater. Res. Technol.* **2021**, *14*, 2382–2393. [CrossRef]
19. Hussain, S.; Rabani, I.; Vikraman, D.; Feroze, A.; Karuppasamy, K.; Haq, Z.U.; Seo, Y.-S.; Chun, S.-H.; Kim, H.-S.; Jung, J. Hybrid design using carbon nanotubes decorated with Mo_2C and W_2C nanoparticles for supercapacitors and hydrogen evolution reactions. *ACS Sustain. Chem. Eng.* **2020**, *8*, 12248–12259. [CrossRef]
20. Liu, Z.; Li, N.; Su, C.; Zhao, H.; Xu, L.; Yin, Z.; Li, J.; Du, Y. Colloidal synthesis of 1t'phase dominated WS_2 towards endurable electrocatalysis. *Nano Energy* **2018**, *50*, 176–181. [CrossRef]
21. Liu, Q.; Li, X.; Xiao, Z.; Zhou, Y.; Chen, H.; Khalil, A.; Xiang, T.; Xu, J.; Chu, W.; Wu, X. Stable metallic 1T-WS_2 nanoribbons intercalated with ammonia ions: The correlation between structure and electrical/optical properties. *Adv. Mater.* **2015**, *27*, 4837–4844. [CrossRef]
22. Vikraman, D.; Hussain, S.; Akbar, K.; Truong, L.; Kathalingam, A.; Chun, S.-H.; Jung, J.; Park, H.J.; Kim, H.-S. Improved hydrogen evolution reaction performance using MoS_2–WS_2 heterostructures by physicochemical process. *ACS Sustain. Chem. Eng.* **2018**, *6*, 8400–8409. [CrossRef]
23. Wu, Z.-Y.; Hu, B.-C.; Wu, P.; Liang, H.-W.; Yu, Z.-L.; Lin, Y.; Zheng, Y.-R.; Li, Z.; Yu, S.-H. Mo_2c nanoparticles embedded within bacterial cellulose-derived 3d n-doped carbon nanofiber networks for efficient hydrogen evolution. *NPG Asia Mater.* **2016**, *8*, e288. [CrossRef]
24. Men, Y.-L.; You, Y.; Pan, Y.-X.; Gao, H.; Xia, Y.; Cheng, D.-G.; Song, J.; Cui, D.-X.; Wu, N.; Li, Y.; et al. Selective co evolution from photoreduction of CO_2 on a metal-carbide-based composite catalyst. *J. Am. Chem. Soc.* **2018**, *140*, 13071–13077. [CrossRef]
25. Gao, W.; Shi, Y.; Zhang, Y.; Zuo, L.; Lu, H.; Huang, Y.; Fan, W.; Liu, T. Molybdenum carbide anchored on graphene nanoribbons as highly efficient all-ph hydrogen evolution reaction electrocatalyst. *ACS Sustain. Chem. Eng.* **2016**, *4*, 6313–6321. [CrossRef]
26. Huang, Y.; Gong, Q.; Song, X.; Feng, K.; Nie, K.; Zhao, F.; Wang, Y.; Zeng, M.; Zhong, J.; Li, Y. Mo_2C nanoparticles dispersed on hierarchical carbon microflowers for efficient electrocatalytic hydrogen evolution. *ACS Nano* **2016**, *10*, 11337–11343. [CrossRef] [PubMed]
27. Fan, M.; Zheng, Y.; Li, A.; Ma, Y.; Huo, Q.; Qiao, Z.A.; Dai, S. Sprout-like growth of mesoporous mo2c/nc nanonetworks as efficient electrocatalysts for hydrogen evolution. *ChemCatChem* **2018**, *10*, 625–631. [CrossRef]
28. Cui, W.; Cheng, N.; Liu, Q.; Ge, C.; Asiri, A.M.; Sun, X. Mo_2C nanoparticles decorated graphitic carbon sheets: Biopolymer-derived solid-state synthesis and application as an efficient electrocatalyst for hydrogen generation. *ACS Catal.* **2014**, *4*, 2658–2661. [CrossRef]
29. Tang, C.; Sun, A.; Xu, Y.; Wu, Z.; Wang, D. High specific surface area Mo_2C nanoparticles as an efficient electrocatalyst for hydrogen evolution. *J. Power Sources* **2015**, *296*, 18–22. [CrossRef]

30. Hussain, S.; Zaidi, S.A.; Vikraman, D.; Kim, H.-S.; Jung, J. Facile preparation of molybdenum carbide (Mo_2C) nanoparticles and its effective utilization in electrochemical sensing of folic acid via imprinting. *Biosens. Bioelectron.* **2019**, *140*, 111330. [CrossRef]
31. Vikraman, D.; Hussain, S.; Patil, S.A.; Truong, L.; Arbab, A.A.; Jeong, S.H.; Chun, S.-H.; Jung, J.; Kim, H.-S. Engineering $MoSe_2/WS_2$ hybrids to replace the scarce platinum electrode for hydrogen evolution reactions and dye-sensitized solar cells. *ACS Appl. Mater. Interfaces* **2021**, *13*, 5061–5072. [CrossRef]
32. Lin, H.; Shi, Z.; He, S.; Yu, X.; Wang, S.; Gao, Q.; Tang, Y. Heteronanowires of MoC–Mo_2C as efficient electrocatalysts for hydrogen evolution reaction. *Chem. Sci.* **2016**, *7*, 3399–3405. [CrossRef]
33. Wu, H.B.; Xia, B.Y.; Yu, L.; Yu, X.-Y.; Lou, X.W.D. Porous molybdenum carbide nano-octahedrons synthesized via confined carburization in metal-organic frameworks for efficient hydrogen production. *Nat. Commun.* **2015**, *6*, 6512. [CrossRef] [PubMed]
34. Vikraman, D.; Hussain, S.; Truong, L.; Karuppasamy, K.; Kim, H.-J.; Maiyalagan, T.; Chun, S.-H.; Jung, J.; Kim, H.-S. Fabrication of MoS_2/WSe_2 heterostructures as electrocatalyst for enhanced hydrogen evolution reaction. *Appl. Surf. Sci.* **2019**, *480*, 611–620. [CrossRef]
35. Wang, X.; Sun, P.; Lu, H.; Tang, K.; Li, Q.; Wang, C.; Mao, Z.; Ali, T.; Yan, C. Aluminum-tailored energy level and morphology of$Co_{3-x}Al_xO_4$ porous nanosheets toward highly efficient electrocatalysts for water oxidation. *Small* **2019**, *15*, 1804886.
36. Wang, X.; Zheng, B.; Yu, B.; Wang, B.; Hou, W.; Zhang, W.; Chen, Y. In situ synthesis of hierarchical $MoSe_2$–$CoSe_2$ nanotubes as an efficient electrocatalyst for the hydrogen evolution reaction in both acidic and alkaline media. *J. Mater. Chem. A* **2018**, *6*, 7842–7850. [CrossRef]
37. Hu, Y.; Yu, B.; Ramadoss, M.; Li, W.; Yang, D.; Wang, B.; Chen, Y. Scalable synthesis of heterogeneous W–W_2C nanoparticle-embedded CNT networks for boosted hydrogen evolution reaction in both acidic and alkaline media. *ACS Sustain. Chem. Eng.* **2019**, *7*, 10016–10024. [CrossRef]
38. Wiensch, J.D.; John, J.; Velazquez, J.M.; Torelli, D.A.; Pieterick, A.P.; McDowell, M.T.; Sun, K.; Zhao, X.; Brunschwig, B.S.; Lewis, N.S. Comparative study in acidic and alkaline media of the effects of ph and crystallinity on the hydrogen-evolution reaction on MoS_2 and $MoSe_2$. *ACS Energy Lett.* **2017**, *2*, 2234–2238. [CrossRef]
39. Yin, Y.; Han, J.; Zhang, Y.; Zhang, X.; Xu, P.; Yuan, Q.; Samad, L.; Wang, X.; Wang, Y.; Zhang, Z.; et al. Contributions of phase, sulfur vacancies, and edges to the hydrogen evolution reaction catalytic activity of porous molybdenum disulfide nanosheets. *J. Am. Chem. Soc.* **2016**, *138*, 7965–7972. [CrossRef]